

AO17: Ash detection and characterisation in IASI data

Candidate number: 441639

Supervisors: Dr E. Carboni and Dr R. G. Grainger

Word count: 4275

Abstract

Methods for the fast detection of volcanic ash using data from satellites have many useful applications, the main real-time application being warning aircraft of the presence of volcanic ash. Previous methods for detecting ash can generate many false positives, while simultaneously missing out genuine detections. In this report a technique is developed to identify ash using the Infrared Atmospheric Sounding Interferometer (IASI). The detection method uses IASI data with no ash and a forward model of spectra with ash in an optimal estimation scheme. This method was applied successfully to ash plumes from several eruptions, as well as being used to retrieve estimates for the area covered and total mass of ash clouds.

1 Introduction

1.1 Importance of detecting ash

Detecting volcanic ash in the atmosphere is important for a number of reasons, chief among them is that volcanic ash is an aviation hazard [1], which can potentially cause engine failure. Volcanic ash in the atmosphere, and where it falls, also has wide ranging impacts on, for example, agriculture, in particular causing damage to crops and changing the soil properties [2]; inland, affecting plant growth and the composition of lakes [4] [3]; in the ocean, providing micronutrients for phytoplankton [5]. An accurate ash retrieval method would allow better investigation of its impact on the environment.

1.2 Previous detection methods

The most commonly used ash detection method is the split window test (also called the brightness temperature difference (btd) method); the method takes the brightness temperature from two channels: from 10.3-11.3 μm (B_{11}) and from 11.5-12.5 μm (B_{12}), a positive detection is given if the difference between the brightness temperature for these two channels is less than zero [6], i.e. if:

$$B_{11} - B_{12} < 0 \quad (1)$$

This method is quick and can be used with data from instruments with coarse spectral resolution. However the method also gives false positives, from sources including dust aerosols, which it cannot distinguish from ash [7], and clouds [8]. Ash can also be masked by ice or water in the atmosphere [8].

Several more modern techniques have been suggested which use data from hyperspectral instruments, e.g. IASI or AIRS (Atmospheric Infrared Sounder). These include:

Exploiting differences between the shape of spectra with ash and those without, in particular looking at the coefficients for quadratic and linear fits in certain regions of the spectra [9].

Creating a database of reference spectra (containing ash) using observations of volcanic plumes and finding the correlation coefficient between the reference spectra and an observed spectrum, resulting in a positive detection if the coefficient is above a threshold value [10].

Using a sophisticated forward model to simulate spectra in many different conditions (including with aerosols such as ash) and then the

optimal estimation retrieval method to find the most probably state of actual spectra based on these simulations [11].

The method used in this report bears some similarities to some of these methods, e.g. a forward model is used to simulate spectra (though unlike the above method just spectra with ash). The proposed method has the attractive quality of using all information available, and so it should be at least as accurate as the split window test or the method using the shape of the spectra which use the same or less information in a less efficient way.

1.3 IASI

The IASI instrument is on the METOP satellite, which was launched in 2006. The instrument is a Michelson interferometer. Its field-of-view gives light atmospheric cells of about 50 km \times 50 km at nadir. A pixel diameter, i.e. the width of the smallest unit of an image taken by the IASI instrument, of 12 km is used to balance radiometric performance and the likelihood of acquiring valid measurements. What makes advanced retrieval techniques possible to use on the data IASI provides is the number of channels it uses; the IASI instrument has a spectral range of 15.5 to 3.62 μm with a spectral resolution of 0.35 to 0.5 cm^{-1} ; the instrument has 8,400 spectral channels, which is many times more than, for example, the 20 channels of the HIRS instrument IASI is designed to replace. The instrument also has a high radiometric resolution (0.1 to 0.5 K) [17]. As instruments like IASI are a great improvement on the previous atmospheric sounders there is a need for new retrieval techniques which takes advantage of the data they provide.

2 Method

The method used is the one described in Walker, Dudhia, Carboni (2011), where it was applied to the detection of sulphur dioxide and ammonia [13].

Differences in observed spectra can be caused by the presence of ash or by other atmospheric

and surface parameters. The aim of this method is to put more weight for changes in parts of the spectra which are likely to change a lot with ash present and less weight in changes in parts of the spectra which change through other atmospheric variation. It is assumed measured spectra \mathbf{y} can be represented by the forward model F and the total measurement error:

$$\mathbf{y} = F(x_c, \mathbf{u}) + \epsilon_{rnd} + \epsilon_{sys} \quad (2)$$

where the notation from Rodgers (2000) has been used [12]: x_c is the column amount of ash, \mathbf{u} represents the estimate of all other conditions (parameters from the instrument, atmosphere and surface), ϵ_{sys} is the error from uncertainty in these parameters and ϵ_{rnd} is random measurement error from instrument noise. For this report the forward model used is a modified version of RTTOV for IASI (used in ORAC retrievals [18]). Aerosol optical depth (τ) is used to represent the column amount of ash. The forward model can be linearised around a value of aod:

$$\mathbf{y} - F(\tau_0, \mathbf{u}) = \mathbf{K}(\tau - \tau_0) + \epsilon_{rnd} + \epsilon_{sys} \quad (3)$$

where the linearisation point is τ_0 and \mathbf{K} is the Jacobian $\frac{\partial \mathbf{y}}{\partial \tau}$ (where \mathbf{y} is taken to be in brightness temperature). The optimal least squares estimate of τ can then be found:

$$\tau = \tau_0 + \mathbf{g}^T(\mathbf{y} - F(\tau_0, \mathbf{u})) \quad (4)$$

where \mathbf{g}^T is the retrieval gain, given by:

$$\mathbf{g}^T = (\mathbf{K}^T \mathbf{S}_\epsilon^{tot-1} \mathbf{K})^{-1} \mathbf{K}^T \mathbf{S}_\epsilon^{tot-1} \quad (5)$$

In this equation $\mathbf{S}_\epsilon^{tot}$ is the covariance matrix of the total error ($\epsilon_{rnd} + \epsilon_{sys}$). If the assumptions used are invalid, especially the assumed value of optical depth, then the result for τ will not be accurate. In these cases it is instead a comparative measure of whether it is likely there is ash present. Later on in the report the method is adapted so that it can be used to accurately retrieve τ . As the signal from variability in non-ash parameters are usually spectrally correlated, if a baseline that accounts for these correlated signals can be found it will allow the signal for ash to stand out; this method allows a baseline to be

found without having to calculate values for each of the relevant parameters. The method can use all channels available to it, channels which don't have a strong ash signal will help establish the baseline. For this report the spectral range used was 650 to 7400 cm^{-1} .

The method used to find $\mathbf{S}_\epsilon^{\text{tot}}$ for this paper is empirical. For an ensemble of data containing N spectra \mathbf{y}_j the total error covariance is:

$$\mathbf{S}_\epsilon^{\text{tot}} \approx \frac{1}{N-1} \sum_{j=1}^N (\mathbf{y}_j - \bar{\mathbf{y}})(\mathbf{y}_j - \bar{\mathbf{y}})^T \quad (6)$$

$\mathbf{S}_\epsilon^{\text{tot}}$ should be created from data that reflects the conditions we expect to be retrieving ash in. The most sensitive detection of ash should be found using an ensemble of data from the specific area and time of year we expect to be using the retrieval. However sacrificing some sensitivity it is possible to use, for example, a global ensemble of data. The important condition is that no ash should be present, which is easily obeyed as ash will only be present after a few specific events. When using an ensemble of data we can also use the average spectrum from the ensemble:

$$\bar{\mathbf{y}} = \sum_{j=1}^N \mathbf{y}_j \quad (7)$$

as an estimate for our fixed forward model $F(\tau_0, \mathbf{u})$. Because of the nature of this method it is not necessary to be selective when picking channels used, at the very least no channel should have a negative effect on retrieval; the one reason to use fewer channels is computational efficiency. If a suitable \mathbf{g}^T and $\bar{\mathbf{y}}$ have been already calculated then this method can be used for the near real-time retrieval of volcanic ash. A positive detection of ash is then defined as:

$$\tau > \tau_{\text{thresh}} \quad (8)$$

where τ_{thresh} is a suitably chosen threshold value.

2.1 Covariance of error matrices and weighting functions

For this report two different covariance of error matrices were used. Both were created from

IASI data encompassing April and May 2009. One, which for convenience will hence forth be referred to as $\mathbf{S}_\epsilon^{\text{ice}}$, took data points from the North Sea, specifically points with latitudes between 45 to 70 and longitudes between -50 to 40. This matrix is ideal for using when detecting ash from the Eijafjallaökull and Grimsvötn eruptions, that occurred in spring 2010 and spring 2011 respectively. The other covariance of error matrix ($\mathbf{S}_\epsilon^{\text{naab}}$) took data from over Eurasia and west Africa between latitudes -10 to 60 and longitudes -10 to 150, initially designed for looking at ash from the Nabro eruption in June 2011. Both matrices were applied to detecting ash in other locations, however with differing success; see appendix B for a detailed comparison.

To find the retrieval gain \mathbf{g}^T the weighting function $\frac{\partial \mathbf{y}}{\partial \tau}$ must first be found. Using the forward model the weighting function can be found for assumed values of ash plume optical depth, height and effective radius. For this report an assumed effective radius of 2 μm was used based on ranges of values recovered from other studies on volcanic ash [14] [15]. After examining some results for various different heights an assumed height with an atmospheric pressure of 300 mb (i.e. a height of approximately 10 km) was chosen to be used for the rest of the report as it allowed sensitive retrieval of ash but kept noise to a minimum. A thorough examination of using an algorithm with multiple assumed heights and/or trying to retrieve the heights of ash plumes would be desirable but is beyond the scope of this report. Aside from the preliminary examination looking at which assumed height to use, the difference in results caused by the different assumptions is also examined (see figure 9).

The weighting function describes how a spectrum is expected to change as aerosol optical depth increases or decreases. However it is expected that different assumed optical depths to generate different weighting functions. In particular a low assumed optical depth should allow for a sensitive detection of thin ash clouds but will not give an accurate retrieval for thick ash clouds, whereas a high assumed optical depth might not allow thin ash clouds to be flagged. This expectation that different assumed optical

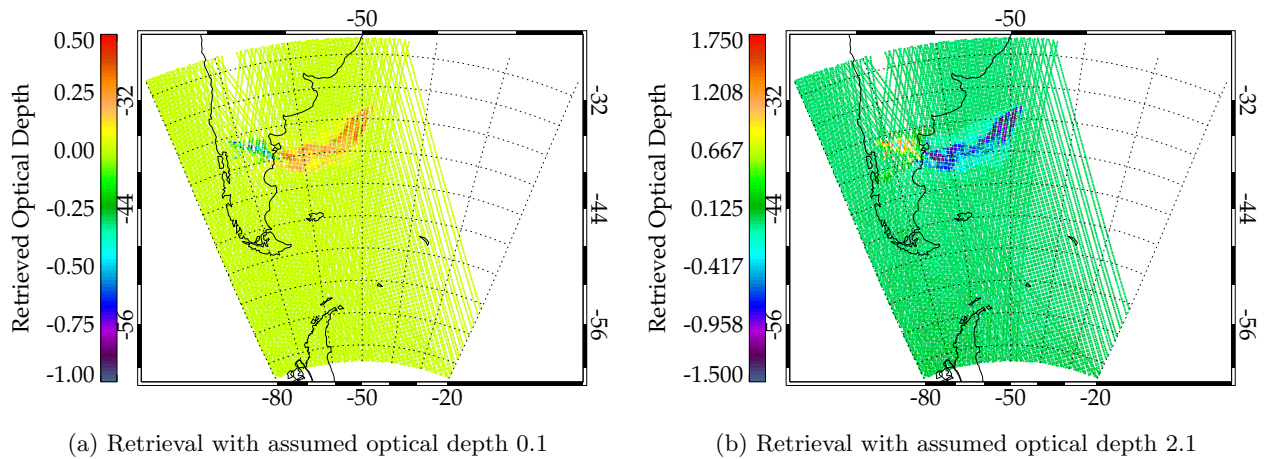


Figure 1: Maps showing the ash plume for the Puyehue eruption on 05/06/2011, each retrieved with different assumed optical depths. For the retrieval with low assumed optical depth the thicker part of the ash plume (the western part, over the land and closer to the volcano) gives a negative result whereas the thinner parts give a positive result. With the retrieval using high optical depth the effect is reversed. Note also that the higher assumed optical depth gives more extreme results.

depths are appropriate for parts of ash clouds is borne out by testing; at it's strongest this effect can mean that parts of the ash cloud for which the assumed optical depth is inappropriate, e.g. thick sections of ash cloud when the forward model is linearised around a small assumed optical depth, can give a strong negative result (see figure 1).

Two solutions to this problem were used. The first aims to find the most accurate retrieval by finding the minimum values of the function

$$(\mathbf{y} - \tau\mathbf{K})^T \mathbf{S}_\epsilon^{tot} (\mathbf{y} - \tau\mathbf{K}) \quad (9)$$

for each spectrum \mathbf{y} using a range of values for τ . The value of τ which gives the minimum of this function is then used as the assumed aerosol optical depth for that spectrum. This function is used as chi-square test between the measured spectra (\mathbf{y}) and the forward model of the spectra (given by $F(\tau) = \tau\mathbf{K}$), weighted by the covariance of error matrix. This method should give the most accurate retrieval of optical depth, however the function used can sometimes be low for low values of τ even though this is not an appropriate value for the retrieval. The use of this function is also very computationally demanding

and so would not be useful for near real time retrieval of ash values.

If a retrieval is run on a pixel with ash assuming a much too high optical depth the result will be small or negative. Similarly if the retrieval is run with a much too low optical depth for that pixel the result will be small or negative. Examples of both of these effects are shown clearly on figure 1. This would suggest that for a range of assumed aerosol optical depths the most appropriate will give the largest result.

To investigate this a set of retrievals can be run on a particular pixel with a range of different assumed optical depths. For pixels of ash there will be a range of optical depths that give very similar results; optical depths outside this range give smaller results, with the more extreme (either higher or lower) optical depths giving the smallest results. An illustration of this is shown in the maps in figure 2. That a range of different assumed optical depths will give the same result is very encouraging for the basic retrieval method. The results fit very well with the expectation that there will be a range of assumed optical depths that are valid for a pixel. It also shows that the further from this range the as-

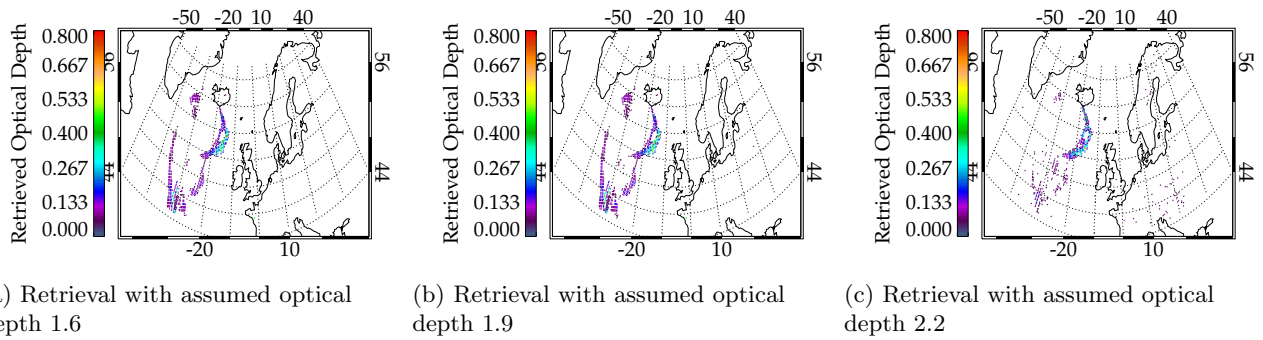


Figure 2: Three maps showing the ash retrieval on the same day (08/05/2010) for the Eyjafjallajökull eruption, each with the threshold value of optical depth 0.05. The difference between the results from maps (a) and (b) are minimal, whereas there is a large difference between maps (b) and (c). This shows how several values of assumed optical depth will give similar results, but not all values.

sumed optical depth is, the smaller the retrieved optical depth will be. This observation therefore strongly suggests that taking the largest value for a range of assumed optical depths will give the best result: not only is the largest result supported by several other similar results, but the other results are varied in a predictable pattern that gives smaller and smaller values (eventually reaching obviously and definitely incorrect retrieved values, i.e. negative results).

Therefore a second method can be proposed. For each pixel the retrieval is run with a range of assumed aerosol optical depths, the result for the pixel is taken to be the maximum value given by these. This method can be referred to as the maximising method. For this report the range of aerosol optical depths used were 0.1, 0.2, 0.3 ... 2.8, 2.9 based on initial observation. This method has the advantage of being reasonably undemanding in terms of computing power, and so is relatively quick to run.

A potential problem with this method is that picking the largest value for every spectra increases the result given for signals without any ash, increasing the noise; however the method also allows for more complicated thresholds. Each pixel has a maximum value retrieved by using a particular assumed aerosol optical depth, that assumed optical depth can be referred to as that pixels ' $a\tau$ ', To put it another way $a\tau$ is the

assumed optical depth that will give the largest result for that individual pixel, the result used in the maximising method. That different pixels have different $a\tau$ can be exploited when creating thresholds. Perhaps predictably the pixels with higher $a\tau$ have relatively larger retrieved optical depths. For example a pixel from an ash plume with a high $a\tau$ will be in the thicker part of the plume and have a high optical depth, similarly a pixel outside the ash plume with high $a\tau$ will give a larger aod than other non-ash pixels. In contrast pixels with low $a\tau$ in the plume will give smaller optical depths, but so will pixels outside the plume. Therefore a lower threshold can be used for pixels with a low $a\tau$, whereas a high threshold is appropriate for pixels with higher $a\tau$. While in theory a different threshold can be set for each different $a\tau$, in practice this would be time consuming and unnecessary, less complicated thresholds can be found that cut out almost all noise, while still leaving the ash pixels. An example of such a threshold might be: pixel is flagged as ash if optical depth > 0.025 for pixels with $a\tau \leq 1.4$ or optical depth > 0.1 for pixels with $a\tau > 1.4$. This kind of threshold can be found by examining both the map of $a\tau$ and the chart comparing $a\tau$ against the retrieved optical depth.

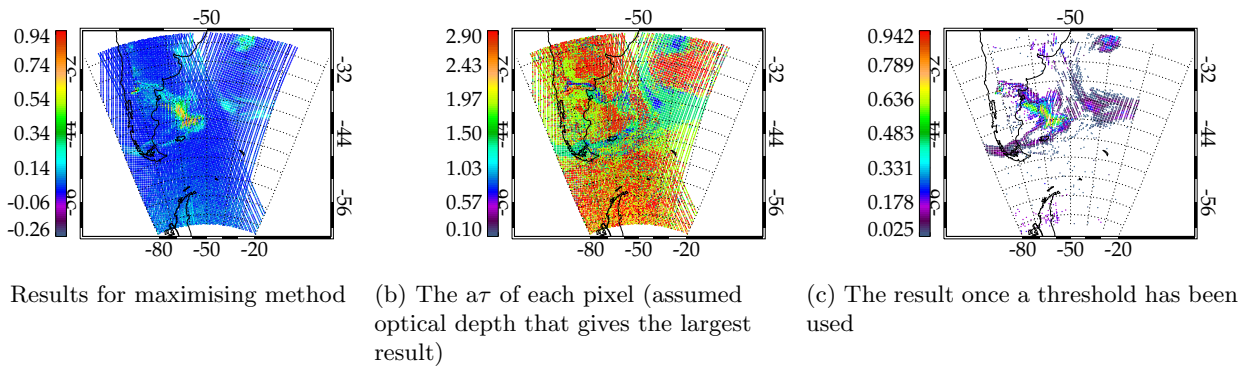


Figure 3: The first map shows results from the maximising method (taken over South America, on 08/06/2011), while the ash cloud is shown there is also a large amount of noise. The second map shows that the pixels of noise tend to have a high $a\tau$, whereas the pixels from the ash cloud that give a low result have a low $a\tau$. The third map is the maximising result after the threshold 'optical depth > 0.025 for $a\tau \leq 1.4$ or optical depth > 0.15 for $a\tau > 1.4$ ', the ash cloud is clear and almost all the noise has been cut out

3 Results

3.1 Plausibility of results

Any other obtained image of the ash clouds looked at will also be dependant on the accuracy of whichever method was used to find it. Because of this uncertainty it is hard to find maps that allow a comparison to judge the accuracy of the method proposed in this report. However it is possible to examine the maps produced by the maximising method and qualitatively examine them as to whether they are plausible re-

sults or not. For example the maps from figure 4. The results found using the maximising method show ash pixels spatially collocated in a plume coming from the volcano. In addition to this the obtained ash cloud develops in a plausible way: the cloud moves steadily, it does not appear to move very rapidly or in many different directions; the changes in the cloud shape are not dramatic and match the movement of the cloud; while the cloud does spread, areas of cloud do not appear and disappear. To sum up the results are strongly consistent with ash coming from the volcano and blown by a wind pattern, making it

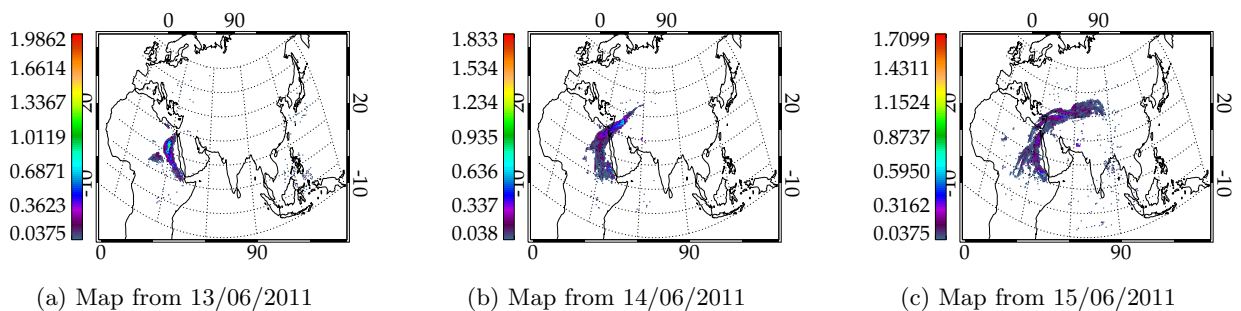


Figure 4: Results from the maximising method. The maps are images created from IASI data after the Nabro eruption, June 2011.

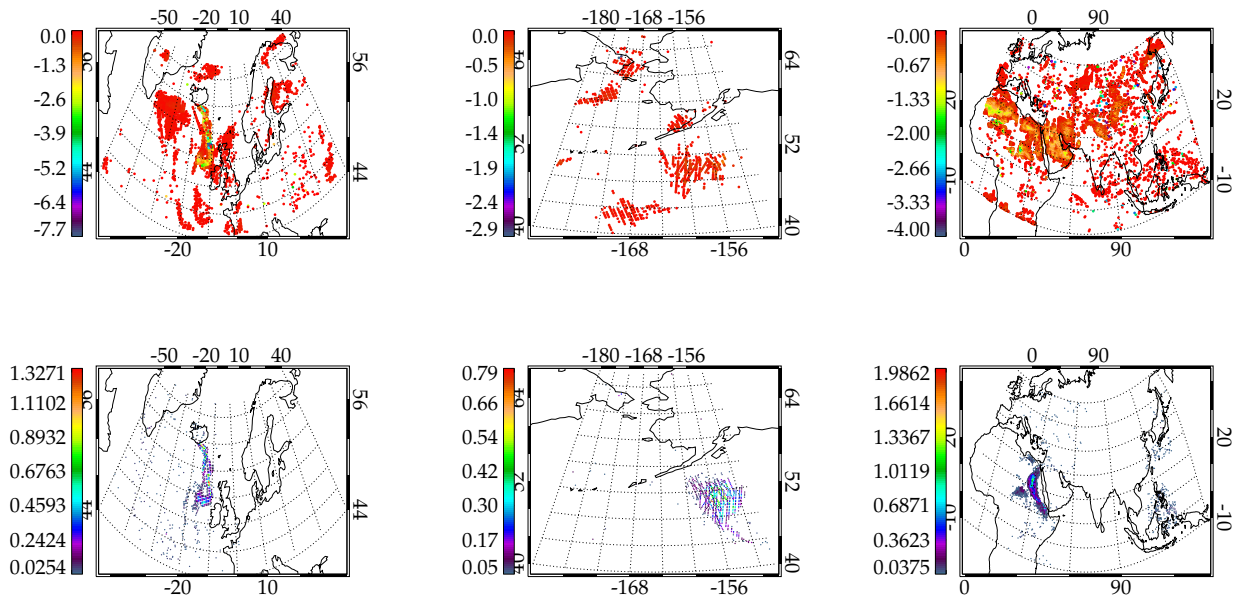


Figure 5: Comparison of brightness temperature difference and maximising method. The first line shows the btd, the second shows the results from the maximising method. The maps in the first column are from 06/05/2010, showing an ash plume from the Eyjafjallajökull eruption; the maps in the second are from 14/07/2008 showing an ash plume from the Okmok eruption; the maps from the third are from 13/06/2011 showing an ash plume from the Nabro eruption

very unlikely these results are not accurate. This is supported by examination of the results from several eruptions.

3.2 Comparison against brightness temperature difference method

The method in this report has several clear advantages over the brightness temperature difference method. This can be shown by qualitatively comparing maps of the same ash plume obtained with the two different methods (see figure 5). While the btd method is sometimes consistent with the maximising method, e.g. when looking at the ash cloud from the Eyjafjallajökull eruption, there are more often than not discrepancies. The btd shows ash in many different locations, some of which being very implausible (i.e. far away from the volcano only a short time after the eruption). The contiguous clouds suggested by the maximising method show ash in locations the btd method doesn't detect any ash, for exam-

ple in the plots over Alaska. In addition to this, whereas the maximising method shows a plausible progression of ash clouds over time, the btd method produces results from consecutive days which appear inconsistent with each other.

3.3 Application to different eruptions

The method was successfully applied to several different eruptions: Okmok, Grimsvötn, Eyjafjallajökull, Nabro and Puyehue. All the applications were successful, though sometimes dependant on covariance of error matrix used (particularly Nabro, see appendix B). A different set of thresholds were applicable to ash from different eruptions; there are two possibilities that might be causing this effect. The first is that the covariance matrices used was more suited to some areas rather than others. For example the optimum threshold for the plume from the Puyehue eruption was higher than that used for the Grimsvötn and Eyjafjallajökull eruptions, this

was using the $\mathbf{S}_\epsilon^{ice}$ matrix which would naturally be more suited to use in the North Atlantic as opposed to the South Atlantic and South America, possibly explaining the discrepancy. The other explanation which might contribute to this effect is the composition of ash in different plumes. Ash from different volcanoes have different compositions and therefore there would be differences in their refractive indices, which would give a different weighting function when using this retrieval. While both of these factors may have had an effect on the retrieval any effect was reasonably minimal, with a different threshold for looking at plumes from different eruptions working well.

3.4 Properties of ash plumes

While the main focus of this report is to test this method's efficiency as an ash flag the method also allows retrieval of properties of the ash. The most obvious and easiest property to retrieve is the size of the ash cloud. As the pixel diameter the IASI instrument uses is known an estimate of the area of the plume size can be found by taking the number of pixels that satisfy the threshold used (i.e. the number of pixels where ash is detected) and multiplying them by a factor based

on pixel size. A factor of 113 was used as the pixel diameter is 12 km so each pixel covers an area of about 113 km². The progression of the size of the ash cloud can then be graphed. As the METOP satellite makes two orbits a day a result for the area the plume covers is given once every twelve hours. Tracking the progression of an ash cloud cannot always be done as there is often areas where there is no data for certain time, as well as this an extremely large area must be observed as plumes can travel long distances.

Another property of the plume which this method allows an estimate of is the column loading of ash, i.e. the total mass of ash from the ground to above the ash plume for a vertical column of unit area. The column loading is proportional to the optical depth and can give us an estimate of the total mass of the ash cloud. The given proportion of optical depth to column loading is approximately

$$m \approx 0.55 \times \tau \quad (10)$$

(see appendix A for the derivation). Applying this to the ash clouds gives an estimate of the mass of ash, again found for every twelve hours.

Using these methods the properties of the plume from the Nabro ash cloud were found, see

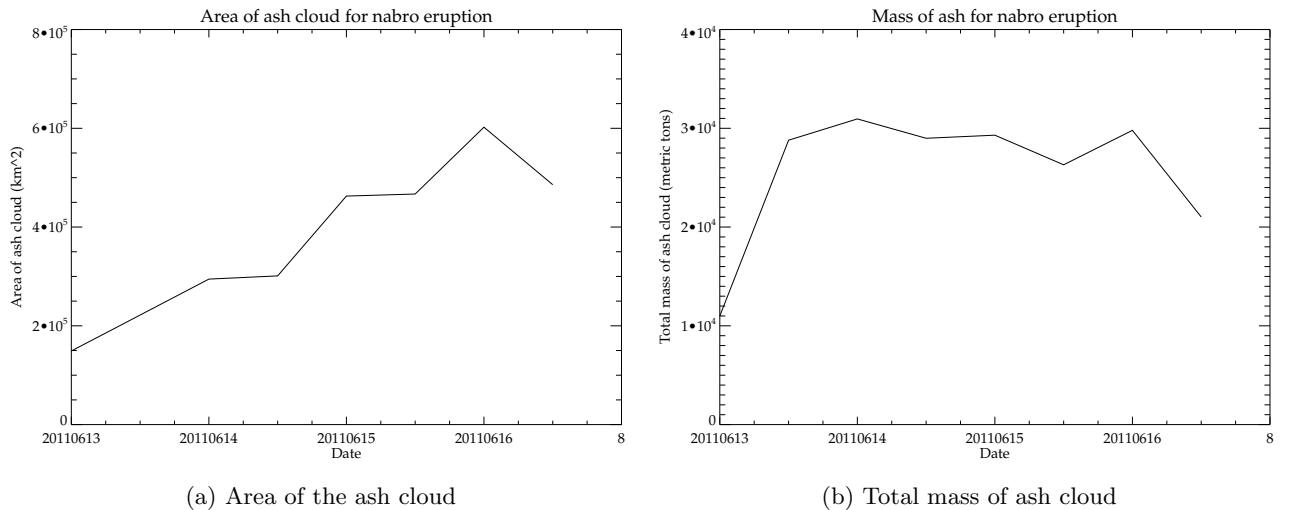


Figure 6: Graphs showing estimates for the change in time of the total mass and area covered of the ash cloud from the Nabro eruption. The first graph shows the evolution of area covered by the plume over four days, the second the evolution of mass over the same four days. Note that while these results allow day to day comparisons they are not expected to be accurate.

figure 6. As would be expected the area of the ash cloud grows over time as the cloud spreads out. The mass of the ash grows rapidly after the initial eruption as more ash is thrown in the air, but starts to decrease as particles drop from the cloud. See figure 4 to see the images of the same ash cloud.

3.5 No fly zone

After the 2010 Eyjafjallajökull eruption a no fly zone was set up over the North Atlantic and Western Europe. Flights were supposedly permitted where ever ash concentrations were less than $2 \times 10^{-3} \text{ g cm}^{-3}$. Using the results in this report it is possible to examine whether the no fly zone that was set up actually reflected the presence of ash.

From comparing the two maps below we can see that the no fly zone mostly in line with the result shown in figure 8, the exception being the portion extended to the east which the results above suggest was unnecessary.

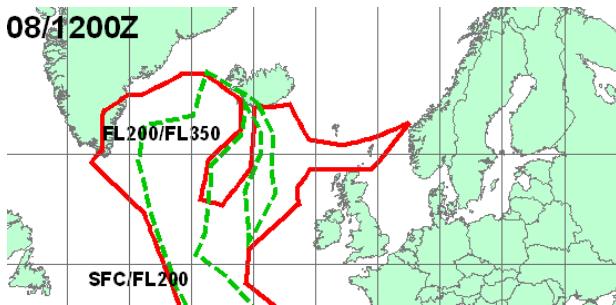


Figure 7: The (red bordered) no fly zone given at 12:00(gmt) on 08/05/2010 due to ash cloud from Eyjafjallajökull [16]

4 Error analysis

There will be two sources of error for the result, the first is error from the data itself, i.e. as determined by the resolution of the IASI instrument. The second is error in our assumptions, in particular the assumptions of height, effective radius and composition of the ash for the forward model. The radiometric resolution of the IASI

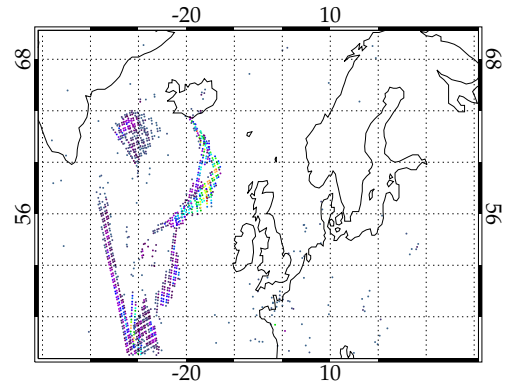


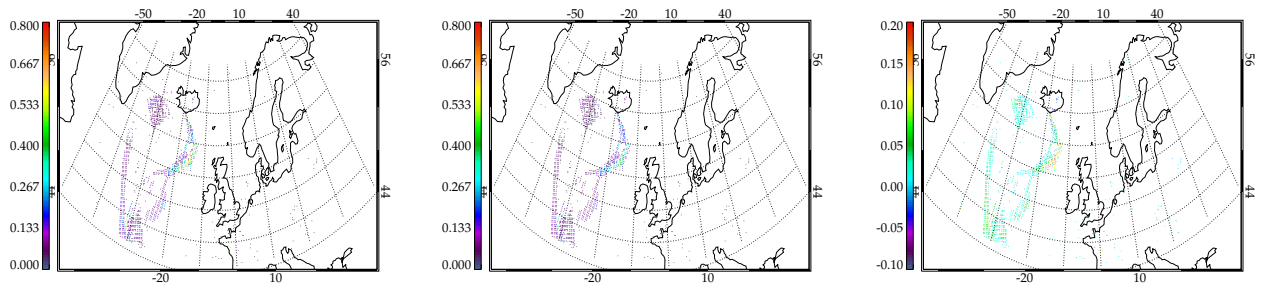
Figure 8: The retrieved ash cloud on the same day (data taken from two orbits, first set of data collected around 10:00-12:00(gmt), the second 21:00-23:00(gmt))

data is 0.1 to 0.5 K [17], the brightness temperature for each spectral line will be a significant amount over 200 K and for every spectra thousands of spectral lines are used; this gives an error in the optical depth of substantially less than 0.01. Whereas changing the assumed height can change the retrieved optical depth by an amount ~ 0.1 (see figure 9, changing the effective radius does not have as large an effect). The composition of the ash and therefore it's refractive index will have an effect on the retrieval results, however this is not expected to be a large effect and the similarity between results for different plumes would support this. Further investigation would be needed to quantify this effect. Overall the first type of error (the systematic error) is negligible compared to the second (error due to assumptions) and the results for optical depth given in this report can be taken as accurate to at least 0.2.

5 Conclusion

In this report a method based on using a forward model the the optimal least squares estimate was used to develop a new flag for ash clouds. This is made possible by the large number of channels hyperspectral instruments like IASI have.

When the method uses the forward model it



(a) Ash optical depth results with the assumed height at 300mb (using maximising method) (b) Ash optical depth results with the assumed height at 750mb (using maximising method) (c) The difference between the two results

Figure 9: Comparison of the aod obtained using the maximising method on the same day, with different assumed heights. The difference between the two varies from pixel to pixel, most have a difference between 0.05 and 0 while some have a difference around 0.1 or even higher.

assumes a height, effective radius and optical depth of the ash cloud. The assumed height is the dominant source of error for the results. Different assumed optical depths can give strongly different results so it is a desirable to use a variation on the method which takes this into account. In this report the variation used was the maximising method which took results for several different assumed optical depths for each pixel and picked the largest.

This was applied very successfully to ash plumes from several different eruptions. This method compared very well to the most commonly used previous method (the brightness temperature difference method), with little to no false positives and more sensitive ash flagging.

The covariance of error matrices used in the method are created from ensembles of IASI data with no ash; in theory when doing a retrieval the covariance of error matrix used should be created from data taken from the same area and time of year which should give the most sensitive retrieval, however in practice using other covariance of error matrices can also work very well. This is convenient as creating the covariance of error matrix is the most computationally demanding part of the retrieval.

Once an ash plume has been flagged properties of the ash plume can then be retrieved, for example, area covered by the ash plume, column

loading of the ash plume and, from the column loading, the total mass of ash in the plume. As this retrieval is quick to run it can be used as a near real-time way of flagging volcanic ash in the atmosphere.

6 Further work

One area more work could be done in is into using different assumed heights and effective radii in the retrieval. This should increase the sensitivity and accuracy of the method. It is also possible that this could then allow values to be retrieved for the height and effect radius of different parts of the ash plume. The differences in refractive index of different compositions of ash and their effect on the retrieval could also be looked into. More work could also be done to investigate using different covariance of error matrices, maybe with the aim of creating a worldwide covariance of error matrix that could be applied to the retrieval in any place at any time of year. This method could also be applied to previous eruptions to try and determine where ash from these eruptions fell using the retrieved area and column loadings of the ash clouds, this would then be helpful in examining the impact volcanic ash has.

Acknowledgements The author would like to thank Dr E. Carboni and Dr R. Grainger for their invaluable support and guidance.

References

- [1] Casadevall, T.J., Delos Reyes, P.J., and Schneider, D.J. The 1991 Pinatubo Eruptions and Their Effects on Aircraft Operations. In: Christopher G. Newhall and Raymond S. Punongbayan (eds.), 1996, Fire and Mud - Eruptions and Lahars of Mount Pinatubo, Philippines: Philippine Institute of Volcanology and Seismology. The University of Washington Press, (p1126).
- [2] Wilson, T., Cole, J., Cronin, S., Stewart, C., Johnston, D., Impacts on agriculture following the 1991 eruption of Vulcan Hudson, Patagonia: lessons for recovery. *Natural Hazards*, Volume: 57 Issue: 2 Pages: 185-212 DOI: 10.1007/s11069-010-9604-8.
- [3] Martin, R. S., Watt, S. F. L., Pyle, D. M., Mather, T. A., Matthews, N. E., Georg, R. B., Day, J. A., Fairhead, T., Witt, M. L. I., Quayle, B. M., Environmental effects of ashfall in Argentina from the 2008 Chaiten volcanic eruption. *Journal of volcanology and geothermal research*, Volume: 184 Issue: 3-4 Pages: 462-472 DOI:10.1016/j.jvolgeores.2009.04.010.
- [4] Watt, S. F. L., Pyle, D. M., Mather, T. A., Day, J. A., Aiuppa, A., The use of tree-rings and foliage as an archive of volcanogenic cation deposition. *Environmental Pollution*, Volume: 148 Issue: 1 Pages: 48-61 DOI: 10.1016/j.envpol.2006.11.007
- [5] Duggen, S., Olgun, N., Croot, P., Hoffmann, L., Dietze, H., Delmelle, P., Teschner, C., The role of airborne volcanic ash for the surface ocean biogeochemical iron-cycle: a review. *Biogeosciences*, Volume: 7 Issue: 3 Pages:827-844 Accession Number: WOS:000276180300003.
- [6] Prata, A.J., Observations of volcanic ash clouds in the 10-12 μ m window using AVHRR/2 data. *International Journal of Remote Sensing*, Volume: 10 Issue: 4-5 Pages: 751-761 Accession Number: WOS:A1989U609700019.
- [7] Simpson, J.J., Hufford, G.L., Servranckx, R., Berg, J., Pieri, D., Airborne Asian dust: case study of long-range transport and implications for the detection of volcanic ash. *Weather and Forecasting*, Volume: 18 Issue:2 Pages: 121-141 DOI: 10.1175/1520-0434(2003)018;0121:AADCSO;2.0.CO;2.
- [8] Simpson, J.J., Hufford, G.L., Berg, J., Pieri, D., Failures in detecting volcanic ash from satellite-based technique. *Remote Sensing of Environment*, Volume: 72 Issue: 2 Pages: 191-217 DOI: 10.1016/S0034-4257(99)00103-0.
- [9] Gangale, G., Prata, A.J., Clarisse, L., The infrared spectral signature of volcanic ash determined from high-spectral resolution satellite measurements. *Remote sensing of the environment*, Volume: 114 Issue: 2 Pages: 414-425 DOI: 10.1016/j.rse.2009.09.007.
- [10] Clarisse, L., Prata, A.J., Lacour, J-L., Hurtmans, D., Clerbaux, C., Coheur, P-F., A correlation method for volcanic ash detection using hyperspectral infrared measurements. *Geophysical research letters*, Volume: 37 Article Number: L19806 DOI: 10.1029/2010GL044828.
- [11] Clarisse, L., Hurtmans, D., Prata, A.J., Karagulian, F., Clerbaux, C., De Maziere, M., Coheur, P-F., Retrieving radius, concentration, optical depth, and mass of different types of aerosols from high-resolution infrared nadir spectra. *Applied Optics*, Volume: 49 Issue: 19 Pages: 3713-3722 Accession Number: WOS:000279403400024.
- [12] Rodgers, C. D.: *Inverse Methods for Atmospheric Sounding*. World Scientific, 2000.
- [13] Walker, J.C., Dudhia, A., Carboni, E., An effective method for the detection of

trace species demonstrated using the MetOp Infrared Atmospheric Sounding Interferometer. Atmospheric Measurement Techniques, Volume: 4 Issue: 8 Pages: 1567-580 DOI: 10.5194/amt-4-1567-2011.

- [14] Grainger, R., Peters, D., Thomas, G., Smith, A., Siddans, R., Carboni, E., Dudhia, A., Measuring Volcanic Plume and Ash Properties from Space, in Remote Sensing of Volcanoes and Volcanic Processes: Integrating Observation and Modelling, Pyle, D. and Mather, T. (eds), The Geological Society Special Publication 270, submitted
- [15] Turco, R.P., Toon, O.B., Whitten, R.C., Hamill, P., Keesee, R.G., The 1980 eruptions of Mount St. Helens' physical and chemical processes in the stratospheric clouds. Journal of Geophysical Research - Oceans and Atmospheres, Volume: 88 Issue: NC9 Pages: 5299-5319 DOI: 10.1029/JC088iC09p05299
- [16] www.metoffice.gov.uk/aviation/vaac/vaacuk_vag.html, Met-Office Volcanic Ash Advisory from London - Issued graphics
- [17] http://smc.cnes.fr/IASI/GP_instrument.htm, CNES IASI instrument specifications
- [18] Thomas, G.E., Carboni, E., Sayer, A.M., Poulsen, C.A., Siddans, R., Grainger, R.G., Oxford-RAL Aerosol and Cloud (ORAC): aerosol retrievals from satellite radiometers. Satellite Aerosol Remote Sensing Over Land, Alexander A. Kokhanovsky and Gerrit de Leeuw (eds), Springer Praxis Books, pgs 193-225, 2009, DOI: 10.1007/978-3-540-69397-0

7 Appendix A: Derivation of relation between optical depth and column loading

In this derivation the first assumption is that the size of ash particles in a plume can be described by a log-normal distribution, i.e. a normal distribution of the logarithm of the particle radii:

$$n(r) = \frac{N_0}{\sqrt{2\pi}} \frac{1}{\sigma r} e^{-\frac{(\ln(r)-\mu)^2}{2\sigma^2}} \quad (11)$$

where, N_0 is the total particles per unit volume, σ is the standard deviation of $\ln(r)$, r is the particle radius and μ is the log mean radius. This can then be used to find an equation for the mass per unit area of a cloud. The volume of all the particles in the cloud is:

$$V = \int_0^\infty \frac{4}{3} \pi r^3 n(r) dr \quad (12)$$

so the mass per unit area of a cloud with ash particles of density ρ and thickness L is:

$$m = \rho \times L \times V = \rho L \frac{4}{3} \pi N_0 r_m^3 e^{\frac{9}{2}\sigma^2} \quad (13)$$

where r_m is the median radius of the distribution. The log normal distribution can also be applied to the formula for the optical depth.

$$\frac{\tau}{L} = \beta^{ext} = \int_0^\infty \pi r^2 Q^{ext} n(r) dr \quad (14)$$

β^{ext} is the volume extinction coefficient, Q^{ext} is the extinction efficiency factor. Putting in the number distribution gives a result for τ .

$$\frac{\tau}{L} = \sqrt{\frac{\pi}{2}} \frac{1}{\sigma} N_0 \int_0^\infty r Q^{ext} e^{-\frac{(\ln(r)-\mu)^2}{2\sigma^2}} \quad (15)$$

Importantly this means optical depth is proportional to number density, therefore we can express optical depth in terms of the extinction coefficient for a particular number density.

$$\tau(N_0) = L \beta^{ext}(N'_0) \frac{N_0}{N'_0} \quad (16)$$

This is useful as $\beta^{ext}(N'_0)$ can be calculated using a Mie scattering code. Rearranging this equation in terms of N_0 and then inserting into the equation for mass per unit area gives:

$$m = \frac{4}{3} \pi \rho \frac{N'_0}{\beta^{ext}(N'_0)} r_m^3 e^{\frac{9}{2}\sigma^2} \times \tau \quad (17)$$

Note that the result is independent of L , the thickness of the cloud. Using the following assumptions for parameters as typical values [14]:

$$r_m \sim 1 \mu\text{m}$$

$$\sigma \approx \ln(1.7)$$

$$\rho \approx 2.4gcm^{-3}$$

Also using the result from a Mie code for many particle scattering to find the extinction coefficient for a particular number density gives

$$m \approx 0.55 \times \tau \quad (18)$$

which can then be applied to the retrieved values of optical depth.

Appendix B: Comparison between covariance matrices

(see figure 10 below)

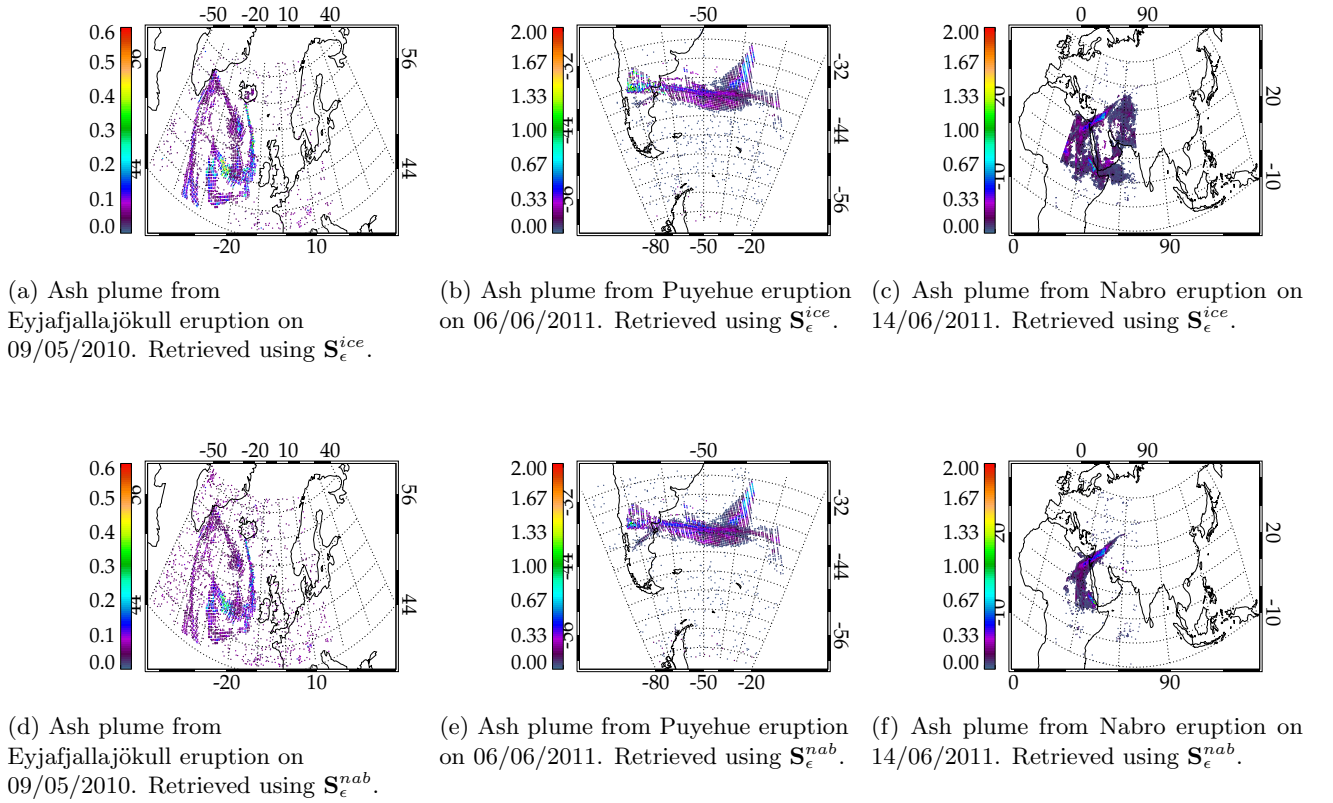


Figure 10: Maps showing a comparison between using different covariant of error matrices (using the same thresholds). The maps showing the plume over the North Atlantic show that the covariance of error matrix more suited to the area ($\mathbf{S}_\epsilon^{ice}$) does generate less noise. Both covariance matrices still worked well though, with only slight differences between retrieved optical depths at thicker parts of the ash cloud. Similarly with the second set of maps, where the only difference is a very slight change in optical depth for some parts of the ash cloud. The maps showing the ash cloud from the Nabro eruption are more dramatically different, with the map using $\mathbf{S}_\epsilon^{ice}$ showing a lot of false positives. This is most likely due to significant amounts of dust in the air which would have been found in the data used to generate \mathbf{S}_ϵ^{ab} but not $\mathbf{S}_\epsilon^{ice}$.